Journal of Materials Chemistry C

Triphenylamine/benzothiadiazole-based Compounds for Non-doped Orange and Red Fluorescent OLEDs with High Efficiencies and Low Efficiency Roll-off

Journal:	*Journal of Materials Chemistry C*
Manuscript ID	TC-ART-01-2021-000249.R1
Article Type:	Paper
Date Submitted by the Author:	05-Mar-2021
Complete List of Authors:	Zhang , Di; Taiyuan University of Technology Yang, Tingting; Shanxi Datong University Xu, Huixia; Taiyuan University of Technology Miao, Yanqin; Taiyuan University of Technology Chen, Run-Feng; Nanjing University of Posts and Telecommunications Shinar, Joseph; Iowa State University, Physics & Astronomy Shinar, Ruth; Iowa State University Wang, Hua; Taiyuan University of Technology Xu, Bingshe; Taiyuan University of Technology, Yu, Junsheng; University of Electronic Science and Technology of China,

ARTICLE

Triphenylamine/benzothiadiazole-based Compounds for Non-doped Orange and Red Fluorescent OLEDs with High Efficiencies and Low Efficiency Roll-off

Received 00th January 20xx,
Accepted 00th January 20xx

DOI: 10.1039/x0xx00000x

Zhang Di [a], Yang Tingting [b], Xu Huixia [a*], Miao Yanqin [a*], Chen Runfeng [c], Shinar Ruth [d], Shinar Joseph [e], Wang Hua [a], Xu Bingshe [a], Yu Junsheng [f]

The long-wavelength materials are key for the development of pure-color and white organic light-emitting devices (OLEDs). An organic molecule, combinating hybridized local electron and charge-transfer (HLCT) and aggregation-induced emission (AIE), not only breaks the 5% external quantum efficiency (EQE) limit but also overcomes emission quenching. Herein, we designed and synthesized four novel donor-acceptor compounds of **TBAN**, **TBT**, **TBAT**, and **TABAT** using triphenylamine (TPA) as the donor, benzothiadiazole (BT) as the acceptor, and anthracene (AN) as a bridge. We found that the emission peaks of **TBAN**, **TBT**, **TBAT** and **TABAT** locate at 596, 615, 580 and 546 nm, respectively. We successfully applied them to non-doped OLEDs, and the resulting devices realize excellent performance. For example, the optimal **TBAN**-based OLEDs show maximum luminance of 74 820 cd/m^2, current efficiency of 12.1 cd/A and maximum EQE of 5.7 % with low roll-off. Additionally, the device with **TBAN** as both emitter and hole-transport material also exhibits high efficiency that is comparable to that of an NPB-based device. This work demonstrates that it is a feasible method to obtain excellent orange and red emitters by employing the BT and TPA based D-A architecture.

Introduction

New-generation emitting materials, such as thermally activated delayed fluorescent (TADF) materials,[1-5] hybridized local electron and charge-transfer (HLCT) emitters, [6-10] and triplet-triplet annihilation (TTA) upconverse fluorophors [11, 12] for low-cost and high-efficiency organic light-emitting devices (OLEDs), have attracted interests in displaying and lighting applications. Currently, most HLCT and TADF emitters with donor-acceptor (D-A) structures are confined to short-wavelength emission, especially in the blue and green. The maximum external quantum efficiency (EQE) for blue TADF-OLEDs has already surpassed 30 %.[13, 14] In contrast, much space is still left for improvement of long-range emitters (orange to red) because of the competition between fluorescence radiative and nonradiative internal conversion rates in the aggregate state, namely aggregation-caused emission quenching (ACQ). [15]

The serious quenching of long-wavelength emitters is an important bottleneck and restricts the development of OLEDs. For example, Zhang et al. reported a series of novel D-A type orange and red fluorescent emitters, which exhibit external quantum efficiency (EQE) of only 3.15% with the emission peak at 592 nm and 2.66% with a 630 nm emission peak. [16] The orange device with an emitter structured by triphenylamine and N, N-diphenylaniline showed a low maximum EQE of 3.42 %.[17] Yang et al. also reported a TADF orange emitter using pyridine-3,5-dicarbonitrile as the core with the electroluminescence (EL) peaking at 600 nm. They achieved a maximum EQE of 9.8 %, [18] much lower than those of blue and green devices. HLCT-based materials with featured D-A structures can achieve reverse intersystem crossing (RISC) by the fast "hot exciton" channel from a high lying triplet state T_m to a high lying singlet state S_n. This unique property endows HLCT-OLEDs with both high EQE and insignificant efficiency roll-off owing to the special hybridized local electron (LE) and charge-transfer (CT) excited states. [19]

To address the ACQ of long-wavelength emitters, it is advisable to design emitters with aggregation-induced emission (AIE), first reported by Tang [20] and successfully applied in many fields. [21, 22] AIE refers to an interesting luminescent phenomenon that nonfluorescent or weakly fluorescent molecules in solutions are induced to emit strong photoluminescence (PL) in aggregate form. The design of long-wavelength emitters integrating both HLCT and AIE features is an effective way to improve the roll-off efficiency [23, 24].

Anthracene (AN) is an attractive building block for high-efficiency fluorescent and electron-transport materials owing

[a] Key Laboratory of Interface Science and Engineering in Advanced Materials, Ministry of Education, Taiyuan University of Technology, Taiyuan 030024, China. E-mail: xuhuixia@tyut.edu.cn; miaoyanqin@tyut.edu.cn
[b] Shanxi Province Key Laboratory of Microstructure Functional Materials Institute of Solid State Physical, School of Physics and Electronic Science, Shanxi Datong University, Datong, 037009, China
[c] Key Laboratory for Organic Electronics and Information Displays & Institute of Advanced Materials, Nanjing University of Posts & Telecommunications, Nanjing 210023, China
[d] Microelectronics Research Canter and Electrical & Computer Engineering Department, Iowa State University, Ames, IA 50011, USA.
[e] Ames Laboratory, USDOE and Physics & Astronomy Department, Iowa State University, Ames, IA 50011, USA.
[f] State Key Laboratory of Electronic Thin Films and Integrated Devices, School of Optoelectronic Science and Engineering, University of Electronic Science and Technology of China (UESTC), Chengdu, 610054, PR China
† Footnotes relating to the title and/or authors should appear here.
Electronic Supplementary Information (ESI) available: Synthetic procedures, chemical characterization data, thermal stability data, theoretical characterization, CV, transient PL decay spectra, AIE natures, device energy level diagram and carrier transport abilities. See DOI: 10.1039/x0xx00000x

to its outstanding photoluminescence (PL) and EL characteristic.[25, 26] In this work, to attain red emission and adjust electron-transport ability, the rigid electron-withdrawing benzothiadiazole (BT) was introduced as an acceptor. In addition, the strong electron-donating triphenylamine (TPA) with unique propeller-like structure was chosen as a donor to effectively reduce π-π stacking, help restrict molecular motion in the aggregate state, and facilitate highly efficient emission in non-doped OLEDs. We designed and synthesized four molecules by combining TPA, BT and AN units, namely **TPA-BT-AN-NA** (**TBAN**), **TPA-BT-TPA** (**TBT**), **TPA-BT-AN-TPA** (**TBAT**) and **TPA-AN-BT-AN-TPA** (**TABAT**). The fabricated OLEDs exhibit strong EL with emission peaks at 597, 608, 604nm, low turn-on voltages of 2.7, 2.4, 2.7 V, maximum current efficiencies of 12.1, 7.3, 9.1 cd/A, and maximum EQEs of 5.7, 4.5, 1.5% for **TBAN**, **TBT** and **TBAT**-based non-doped devices, respectively.

Results and discussion

Synthesis and characterization

All molecules were synthesized mainly by the multi-step Suzuki coupling reactions, as shown in Scheme S1. The chemical structures of the target compounds were characterized by ^{1}H NMR, ^{13}C NMR and mass spectrometry (Supporting Information, ESI†). The thermogravimetric analysis (TGA) and differential scanning calorimetry (DSC) were performed to evaluate the thermal stability, as shown in Fig. S1 (ESI†). The compounds display high thermal stability with decomposition temperature (T_d, with 5% weight loss) of 463 ℃ for **TBAN**, 375 ℃ for **TBT**, 442 ℃ for **TBAT** and 513℃ for **TABAT**, indicating that they can endure high temperature and not decompose during vacuum evaporation. From the DSC curves, the glass transition temperatures (T_gs) were determined to be 100℃ for **TBAN**, 100 ℃ for **TBT**, 162℃ for **TBAT.** No T_g for **TABAT** was observed.

Theoretical simulation and electrochemical properties

DFT (Density functional theory) was used to predict the frontier molecular orbitals of all the molecules. As shown in Fig. 1a, the optimized ground state structures of these four molecules display the nearly coplanar (33°) skeleton of benzene rings on TPA and BT units. The planar structures may result in an overlap distribution of the HOMO and LUMO, which are feasible to form a LE excited state. As expected, the electron density of the highest occupied molecular orbital (HOMO) in the symmetric **TBT** largely disperses over on the whole molecule, while the lowest unoccupied molecular orbital (LUMO) centralizes on the acceptor of BT (Fig. S2, ESI*). The large twisted angles between the BT and AN group are 85° for **TBAN**, 88° for TBAT, and 82/86° for **TABAT**. These large torsions led to well separated HOMOs and LUMOs, which is beneficial to the charge-transfer (CT) state. Additionally, the highly twisted and rigid non-planar structure of these molecules suppresses intermolecular π-π stacking and reduces the concentration of triplet excitons, facilitating highly efficient emission in non-doped fluorescent OLEDs.

The natural transition orbitals (NTO) were calculated to examine the electronic transition features of the lowest excited-state singlet (S_1) and the high-lying triplet properties (Fig.1c and Fig. S3, ESI*). The HLCT characteristic of **TBT** results from S_1 with a large oscillator strength (f=0.4483) and T_2 states. The hole and particle of S_1 present spatial separation with partial overlap, while T_2 exhibits a CT excited state. We further estimated the first ten singlet and triplet states. The corresponding S_1-T_2 energy gap of **TBT** is 0.12 eV and the large difference T_1-T_2 is 0.65 eV. Therefore, RISC process may originate from T_2 to S_1 (Fig. 1d). The hole and particle of $S_0 \rightarrow S_1$ for **TBAN**, **TBAT,** and **TABAT** exhibit a tiny overlap, showing the dominant CT properties, while their high lying T_3 states display hybrid LE and CT states, which result in the HLCT excited state. For **TBAN** and **TBAT**, there are large energy gaps between T_3 and T_1 and negligible gaps between T_2 and T_1. So, small difference gaps between T_3

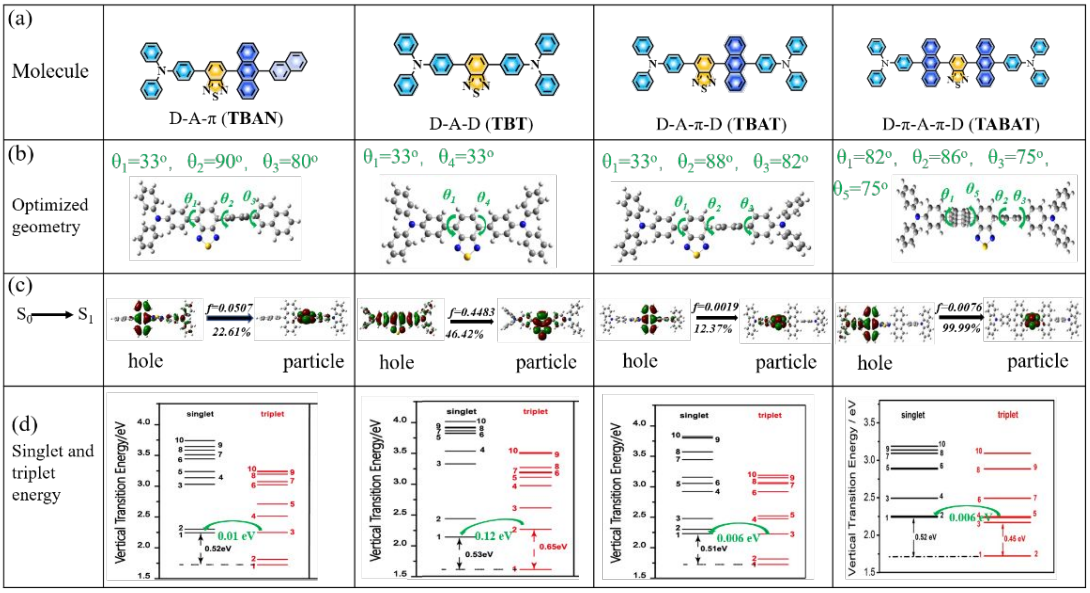

Fig. 1 Molecular structures (a), optimized ground geometries (b), NTOs of $S_0 \rightarrow S_1$ (c) and first ten singlet and triplet energy for the four emitters (d)

and S_1 would be impelled to achieve RISC from T_3 to S_1. For **TABAT**, the energy levels of T_1 and T_2 are nearly equal. The small energy gap is also observed between high-lying T_5 and S_1 (0.006 eV).

The HOMO energy levels were determined to be -5.56 eV for the single-donor **TBAN**, -5.26 eV for **TBT** with D-A-D symmetrical architecture, -5.36 eV for **TBAT** with D-A-π-D configuration, and -5.11 eV for **TABAT** with D-π-A-π-D structure from cyclic voltammetry (CV) curves, in Fig. S4 (ESI*). The shallow HOMO level of **TBAN** can be ascribed to its weak electron-donating ability. From the absorption and emission spectra in DCM, the energy gaps (E_gs) were estimated to be 2.37, 2.28, 2.39, and 2.58 eV, respectively. The LUMO levels were estimated from the E_g and HOMO to be 3.19 eV for **TBAN**, -2.98 eV for **TBT**, -2.97 eV for **TBAT** and -2.53 eV for **TABAT**.

Table 1 The photophysical data and thermal stability of the compounds in this work

compound	λ_{abs} [a] / nm	λ_{em} [a] / nm	λ_{em} [b] / nm	PLQY[c] / %	T_d [d] /℃	T_g [e] / ℃	E_{HOMO} / eV
TBAN	377, 399, 438	560	595	33.4	463	100	-5.56
TBT	460	600	615	35.7	375	100	-5.26
TBAT	377, 395, 447	560	576	25.5	442	162	-5.36
TABAT	393	546	536	18.4	512	—	-5.11

[a] in toluene solution; [b] in thin film; [c] absolute PL quantum yield in film; [d] the temperature at the 5% weight loss; [e] the glass transition temperature

Crystal Structures

Single crystals of **TBAT** and **TBT** were obtained by slow evaporation of their dichloromethane/ methanol mixture solution. X-ray single-crystal diffraction analysis shows that AN group for **TBAT** is highly twisted with angles of 78.38° and 86.94° between adjacent BT and benzene ring (Fig. 2a), which can prevent close intermolecular π-π stacking, in agreement with the DFT calculations. From the stacking distance of **TBAT** (6.21 Å) and for **TBT** (5.71 Å), there is no efficient π-π packing, indicating weak intermolecular interactions. This would be beneficial to relieve fluorescence quenching by aggregation in the film state and construct simplified non-doped OLEDs.

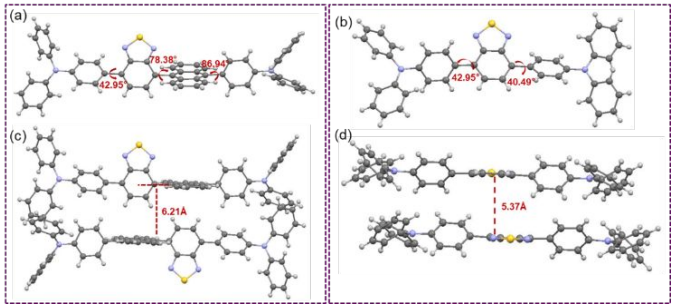

Fig. 2 Single-crystal structures (a), (b) and π-π packing (c), (d) for **TBAT** and **TBT**

Photophysical properties

In the UV/vis absorption spectra (Fig. 3), the well-resolved absorption bands of **TBAN**, **TBAT** and **TBABT** at ~300 nm are characteristics of the π-π* transition of the anthracene moiety, [27, 28] which disappears for **TBT**. The absorption bands at 400-450 nm can be attributed to the intramolecular charge-transfer (ICT) transition from donor to accepter in toluene solution. The ICT absorption peak for **TBT** is red shifted to 460 nm, suggesting a strong CT excited state. For **TABAT**, no ICT transition band was observed due to the broken conjugation between TPA and BT caused by the large torsion angles.

TBABT, **TBAN**, **TBAT** and **TBT** exhibit green to red emission with peaks at 546, 560, 560 and 600 nm in dilute toluene solution, respectively. **TBABT** exhibits a highly blue-shifted emission spectrum, implying a weak ICT transition. The photoluminescence quantum yields (PLQYs) were measured to be 5.7% for **TBABT,** 30.2 % for **TBAN** and 21.5 % for **TBAT**. We couldn't get the PLQY of **TQT** in toluene due to solvent effect. The radiative decay constant (k_r) of S_1 states were estimated by the absorption spectra to be 3.86×10^8 s^{-1} for **TBAN**, 4.80×10^8 s^{-1} for **TBT**, 2.79×10^8 s^{-1} for **TBAT** and 1.15×10^8 s^{-1} for **TBABT** (Equations S1 and S2, ESI*). [29] The four compounds **TBAN**, **TBT**, **TBAT**, and **TBABT** in toluene exhibit monoexponentially decay with lifetimes τ_s of 4.53, 6.07, 3.86 and 2.13 ns, respectively (Fig. S5, ESI*). No delayed component was observed, suggesting the emission exclusively originates from S_1 decay. In neat films, these compounds generate stronger emission than in toluene solution with peaks at 595, 615, 576 and 536 nm with PLQYs of 33.4, 35.7, 25.5 and 18.4 %, respectively.

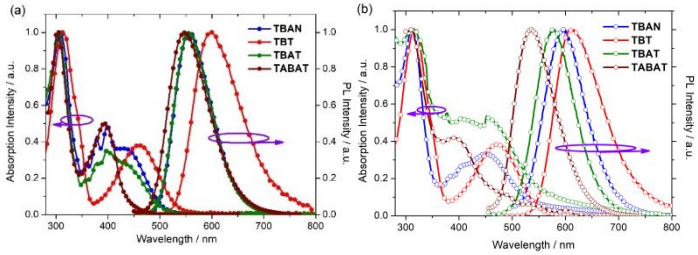

Fig. 3 The UV-Vis absorption and PL of **TBAN, TBT, TBAT** and **TABAT**, in toluene (a) and films (b)

As shown in Fig. S6 (ESI*), the absorption spectra display no obvious changes as the solvent polarity increases, suggesting a rather small dipole moment change at the ground state in different solvents. The emission spectra (Fig. S7) show a significant redshift of 133 nm for **TBAN**, 130 nm for **TBT**, 126 nm for **TBAT** and 107 nm for **TBABT** as the solvent polarity varies from the low-polarity hexane to high-polarity acetonitrile. Such a large red-shift demonstrates a strong ICT in the excited state. While, the red-shift of **TBABT** is the smallest, further suggesting a weak ICT state. To better understand the solvatochromic effect and the excited state properties, the Lippert-Mataga solvatochromic models were constructed. [30, 31] The results present two-section linear correlations (Fig. S8, ESI*). The line with the small slopes is due to the LE-like excited states with

lower excited state dipole moment (μ_e), while the large slopes in high polarity solvents are from the CT-dominant excited states with the greater μ_e.

Emission behaviours in aggregated state

The emission in the aggregate state was investigated in 1×10^{-5} M THF/water solutions with the water fraction (vol%) varying from 0 to 99%. All compounds exhibit changing UV-vis absorption and fluorescence spectra depending on the water fraction. At low water volume (0-60 or 70%), the emission spectra of **TBAN**, **TBT**, **TBAT**, and **TABAT** exhibit a red shift with decreased intensity, as shown in Fig. 4 and S9. This result shows that the ICT excited state is highly dependent on the solvent polarity. At high water percentage from 60 to 99 %, the emission intensity gradually recovers and the emission peaks present blue shifts. The solubility of **TBAN**, **TBT**, **TBAT**, and **TABAT** tend to decline with increasing water percentage. In that case, the molecules incline to aggregate, the molecular rotation of the TPA unit is suppressed, and the radiative decay constants are enhanced. [32, 33] Therefore, the emission is mainly affected by THF polarity at low water volume, while the AIE dominates over the solvent polarity. Consequently, these molecules could be used in non-doped fluorescent OLEDs.

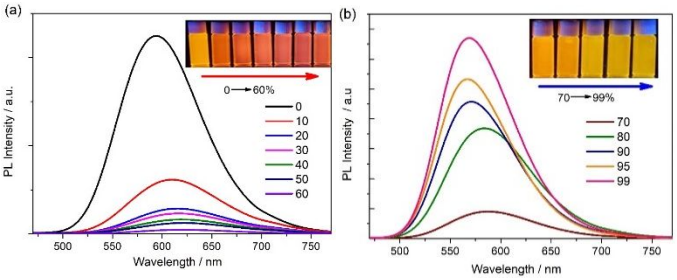

Fig. 4 The emission spectra of **TBAT** in THF/water with different water fractions

Electroluminescence performances

The interesting excited state nature of the synthesized molecules inspired us to investigate their potential applications as emitters in doped and non-doped OLEDs. First, the doped devices' structures were (ITO) /MoO_3 (3 nm)/NPB (30 nm)/TCTA (10 nm)/CBP: 30 wt% emitters (20 nm)/$Bepp_2$ (50 nm)/LiF (1 nm)/Al (100 nm). The emitting layers were **TBAN**, **TBT**, **TBAT**, and **TABAT** doped in CBP (4,4'-Bis(9H-carbazol-9-yl)biphenyl) host; the corresponding doped devices are denoted as D1, D2 D3 and D4. The devices' energy-level diagram and molecular structures are presented in Fig. S10 (ESI*). The EL spectra, current density-voltage-luminance (*J-V-L*) characteristics, current efficiency-luminance-power efficiency (*CE-L-PE*) plot and external quantum efficiency-luminance (*EQE-L*) curves were depicted in Fig. 5 and EL data were summarized in Table 2.

All doped devices show low turn-on voltages of 2.7-2.8 V. The EL peaks are at 576, 604, 576 and 560 nm, slightly redshifted than from the PL peaks in toluene solution due to the different aggregate states (Fig. S11 ESI*). No emission from CBP was observed, indicating complete energy transfer from host to the emitter. The **TBAN**-based device D1 exhibits the highest maximum current efficiency (CE_{max}) of 12.8 cd/A, still remaining at 9.1 and 12.0 cd/A at 100 and 1000 cd/m^2. The maximum EQE reached 4.8%, which is close to the 5% limit. The **TBT**-based device D2 displays red emission peaking at 604 nm, and achieved the best performance with a maximum luminance (L_{max}) of 1 3 690 cd/m^2, CE_{max} of 9.1 cd/A, a maximum power efficiency (PE_{max}) of 9.6 lm/W and a maximum EQE of 5.0 %. The device D3 reached superior high luminance of 42 020 cd/ m^2.

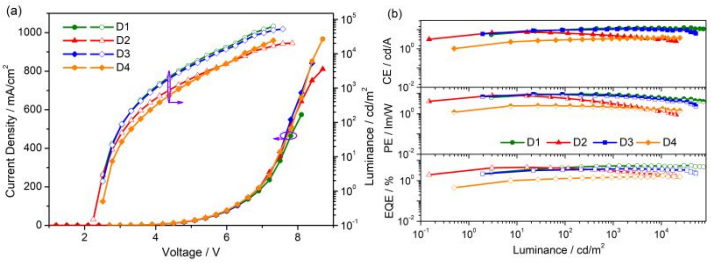

Fig. 5 (a) *J-V-L* curves; (b) CE, PE and *EQE-L* curves of doped devices D1-D4

The unique AIE properties and excellent performances of the doped devices inspired us to fabricate and evaluate non-doped devices with the configuration ITO /MoO_3 (3 nm)/NPB (30 nm)/TCTA (10 nm)/emitter (20 nm)/$Bepp_2$ (50 nm)/LiF (1 nm)/Al (100 nm) (**TBAN** for N1, **TBT** for N2, **TBAT f**or N3 and **TABAT** for N4). The EL characterizations for all non-doped devices, including *J-V-L* and *CE, PE, EQE-L* curves are shown in Fig. 6. The non-doped OLEDs turned on at lower voltages of 2.4-2.8 V and exhibited orange to red EL with peaks from 580 to 608 nm. All non-doped devices show very stable EL spectra, which are almost overlapped from 3 to 7 V (Fig. S12). The Commission Internationale de L'Eclairage (CIE) coordinates are (0.55, 0.44), (0.59, 0.39), (0.50, 0.48) and (0.49. 0.47) for the **TBAN**, **TBT**, **TBAT** and **TABAT** based devices at 5 V, respectively, which are in the yellow to red region in the 1931 CIE coordinates graph. **TABN**-based device N1 reached a L_{max} of 78 420 cd/m^2 at 8 V, a CE_{max} of 12.1 cd/A, a PE_{max} of 14.8 lm/W, and a maximum EQE of 5.7 %, beyond the theoretical EQE_{max} (5%) of conventional fluorescent OLEDs. The device N3 reached L_{max} of 52 390 cd/m^2 at 8.4 V, CE_{max} of 10.7 cd/A, PE_{max} of 9.2 lm/W, and maximum EQE of 4.0 %. The performances of these two orange devices are better than the reported ones at the same peak emission. [35-38] The radiative exciton utilization (η_r) for all devices were calculated to be 85.3, 70.0, 78.4 and 48.9 %.[9, 28] No efficiency roll-off is observed for device N1 before the luminance reached 1000 cd/m^2. Thus, all the non-doped devices display better performance than the doped ones. This indicates that the unique AIE nature of the emitters can effectively suppress the quenching behaviour in aggregate states and improve efficiency.

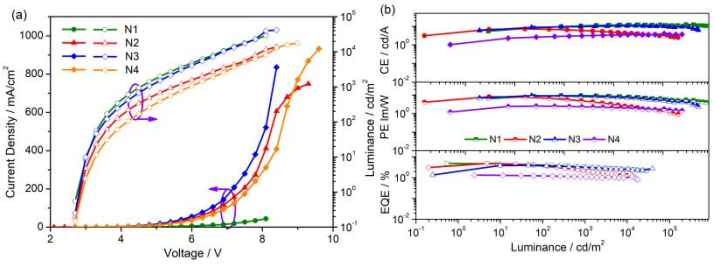

Fig. 6 (a) *J-V-L* curves; (b) *CE, PE* and *EQE-L* curves of doped devices N1-N4

Table 2 Performance of doped and non-doped devices based synthesized emitters

Device	λ_{max}[a] / nm	V_{on}[b] / V	L_{max}[c] /cd/m²	CE_{max}[d] / cd/A	PE_{max}[e] / lm/W	CIE (x, y)	EQE_{max}[f] / %	Performances at 100 / 1000 cd/m²		
								CE	PE	EQE
D1	576	2.7	28890	12.8	9.4	(0.46, 0.45)	4.8	9.1/12.0	9.9/9.6	4.1/3.3
D2	604	2.7	13690	9.1	9.6	(0.56, 0.40)	5.0	7.2/5.7	7.0/4.4	3.5/1.9
D3	576	2.8	42020	10.7	11.2	(0.49, 0.47)	3.9	8.7/10.2	9.6/8.5	3.9/3.1
D4	560	2.8	17590	3.7	3.9	(0.37, 0.44)	1.32	2.5/2.9	2.4/2.2	1.1/1.0
N1	596	2.7	78420	12.1	14.8	(0.55, 0.44)	5.7	11.7/9.0	11.2/6.5	4.7/5.7
N2	608	2.4	20250	7.3	8.0	(0.59, 0.39)	5.0	6.2/5.2	6.3/3.3	4.0/3.0
N3	580	2.6	52390	10.7	9.2	(0.50, 0.48)	4.0	9.3/10.1	9.3/7.2	3.3/3.7
N4	592	2.8	24340	4.1	2.5	(0.49, 0.47)	1.8	2.9/3.4	2.4/2.1	1.2/1.4
G1	587	3.2	68450	14.3	10.7	(0.53, 0.46)	5.7	12.3/14.2	9.7/9.2	5.0/5.7

[a] the EL peaks at 5 V; [b] the voltage at 1cd/m²; [c] the maximum luminance; [d] the maximum current efficiency; [e] the maximum power efficiency; [f] the maximum external quantum efficiency

comparatively, the EL performance of both non-doped and doped devices based on **TBAN** and **TBT** are superior to those of **TBAT** and **TABAT**. Therefore, single-carrier devices were fabricated to understand the underlying cause. As shown in Fig. S13, both hole-only (HOD) and electron-only devices (EOD) based on **TBAN** and **TBT** display better bipolar-carrier transport abilities. We also found that all molecules possess excellent hole-transport abilities. As expected, these compounds can act as both hole-transport and emitting materials in one single device. So, the devices with the structure of ITO/ MOO_3 (3 nm) / **TBAN** (30 nm) TCTA (10 nm)/**TBAN** (20)/ $Bepp_2$ (50 nm)/LiF (1 nm) /AL (100 nm) (**TBAN** for device G), achieved L_{max} of 68450 cd/m² at 8 V, CE_{max} of 14.3 cd/A, PE_{max} of 10.7 lm/W and maximum EQE of 5.7 %, comparable to the device with NPB as the hole-transport materials (Fig. 7). In addition, device G1 shows no roll-off before 1000 cd/ m². This result is mainly attributed to the balanced charge-transfer properties that resulted from the excellent hole-transport ability of **TBAN**. Meanwhile, the simple OLEDs could reduce exciton quenching at interfaces because of the reduced number of functional layers.

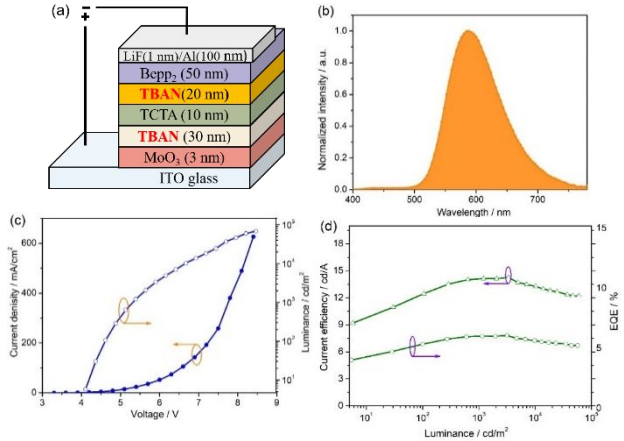

Fig. 7 Devices G1 structure (a), EL spectra, *J-V -L* curves (c) and CE-L-EQE curves (d)

Conclusions

In this work, four molecules with D-A-π, D-A-D, D-A-π-D and D-π-A-π-D structures were designed and synthesized by manipulating the linkages triphenylamine, benzothiadiazole and anthracene. All four molecules show AIE emission behavior and present high PLQY in films. Further, doped and non-doped devices were fabricated to investigate their EL performance. The devices achieved excellent performance and negligible efficiency roll-off. The non-doped **TBAN**-based device exhibited excellent orange emission with L_{max} of 78 420 cd/m² at 8 V, CE_{max} of 12.1 cd/A, PE_{max} of 14.8 lm/W and maximum EQE of 5.7 %. Furthermore, the device based on **TBAN** as both hole-transport and emitting material reached high efficiency, comparable to NPB. The result of our work revealed that the novel anthracene derivatives with AIE possess a huge potential to further simplify the OLED structure and improve the performance of orange-red OLEDs.

Conflicts of interest

There are no conflicts to declare.

Acknowledgements

This work was financially supported by National Natural Scientific Foundation of China (61705156, 21071108, 60976018, 61605138); Natural Science Foundation of Shanxi Province (201901D111108); Key R&D program of Shanxi Province (International Cooperation, 201903D421087, 201903D121100); Shanxi Scholarship Council of China (2020-049; the open research found of key laboratory for organic electronics and information displays. Ames Laboratory is operated by Iowa State University for the US Department of Energy under Contract No. DE-AC 02-07CH11358.

Notes and references

1 H. Uoyama, K. Goushi, K. Shizu, H. Nomura, C. Adachi, *Nature*, 2012, **492**, 234-238.

2 T. Nishimoto, T. Yasuda, S. Y. Lee, R. Kondo, C. Adachi, *Mater. Horiz.* 2014, **1**, 264-269.

3 C. S. Oh, D. S. Pereira, S. H. Han, H.-J. Park, H. F. Higginbotham, A. P. Monkman, J. Y. Lee, *ACS Appl. Mater. Interfaces* 2018, **10**, 35420-35429.

4 J.-X. Chen, W.-W. Tao, Y.-F. Xiao, S. Tian, W.-C. Chen, K. Wang, J. Yu, F.-X. Geng, X.-H. Zhang, C.-S. Lee, *J. Mater. Chem. C* 2019, **7**, 2898-2904.

5 X. Zheng, R. Huang, C. Zhong, G. Xie, W. Ning, M. Huang, F. Ni, F. B. Dias, C. Yang, *Adv. Sci.* 2020, 1902087

6 W. Li, Y. Pan, R. Xiao, Q. Peng, S. Zhang, D. Ma, F. Li, F. Shen, Y. Wang, B. Yang, Y. Ma, *Adv. Funct. Mater.* 2014, **24**, 1609-1614.

7 Chen, W.-C.; Yuan, Y.; Ni, S.-F.; Tong, Q.-X.; Wong F.-L.; Lee, C.-S. *Chem. Sci.* 2017, **8**, 3599-3608.

8 W. Zeng, Y. Zhao, W. Ning, S. Gong, Z. Zhu, Y. Zou, Z.-H. Lu, C. Yang, *J. Mater. Chem. C* 2018, **6**, 4479-4484.

9 X. Tang, Q. Bai, Q. Peng, Y. Gao, J. Li, Y. Liu, L. Yao, P. Lu, B. Yang, Y. Ma, *Chem. Mater.* 2015, **27**, 7050-7057.

10 S. Xue, Qiu X., S. Ying, Y. Lu, Y. Pan, Q. Sun, C. Gu, W. Yang, *Adv. Optical Mater.* 2017, 1700747.

11 R. Ieuji, K. Goushi, C. Adachi, *Nat. Commun.* 2019, **10**, 5283.

12 G. Xie, L. Ding, *Science Bulletin*, 2020, **65**, 1780-1782.

13 C. Li, C. Duan, C. Han, H. Xu, *Adv. Mater.* 2018, **30**, 1804228.

14 C.-C Peng, S.-Y. Yang, H.-C. Li, G.-H. Xie, L.-S. Cui, S.-N. Zou, C. Poriel, Z.-Q. Jiang, L.-S. Liao, *Adv. Mater.* 2020, 2003885.

15 N. Prachumrak, S. Pojanasopa, S. Namuangruk, T. Kaewin, S. Jungsuttiwong, T. Sudyoadsuk, V. Promarak, *ACS Appl. Mater. Interfaces* 2013, **5**, 8694-8703.

16 Y. Zhang, Z. Chen, J. Song, J. He, X. Wang, J. Wu, S. Chen, J. Qu, W.-Y. Wong, *J. Mater. Chem. C* 2019, **7**, 1880-1887.

17 C. Zhou, X. Zhang, G. Pan, X. Tian, S. Xiao, H. Liu; S. Zhang, B. Yang, *Org. Electron*. 2019, **75**, 105414

18 Z. Chen, Z. Wu, F. Ni, C. Zhong, W. Zeng, D. Wei, K. An, D. Ma, C. Yang, *J. Mater. Chem. C* 2018, **6**, 6543-6548

19 Y. Gao, S. Zhang, Y. Pan, L. Yao, H. Liu, Y. Guo, Q. Gu, B. Yang, Y. Ma, *Phys. Chem. Chem. Phys.* 2016, **18**, 24176-24184.

20 J. Luo, Z. Xie, J. W. Y. Lam, Lin Cheng, B. Z. Tang, H. Chen, C. Qiu, H. S. Kwok, X. Zhan, Y. Liu, D. Zhu, *Chem. Commun.* 2001, **18**, 1740-1741.

21 S. Xu, Y. Duan, B. Liu, *Adv. Mater.* 2020, **32**, 1903530

22 H. Zhou, M. H. Chu, B. Z. Tang, J. Xu, J. *Polym. Chem.* 2019, **10**, 3822

23 A. Nicol, W. Qin, R. T. K. Kwok, Z. J. Burkhartsmeyer, M. Zhu, H. Su, W. Luo, J. W. Lam, Y. J. Qian, K. S. Wong, B. Z. Tang, *Chem. Sci.* 2017, **8**, 4634-4643.

24 J. Li, R. Zhang, Z. Wang, B. Zhao, J. Xie, F. Zhang, H. Wang, K. Guo, *Adv. Optical Mater.* 2018, **6**, 1701256.

25 L. Xing, Z-L. Zhu, J. He, Z. Qiu, Z. Yang, D. Lin, W-C. Chen, Q. Yang, S. Ji, Y. Huo, C-S. Lee, *Chem. Eng. J.* 2020, doi: https://doi.org/10.1016/j.cej.2020.127748

26 B. Chen, B. Liu, J. Zeng, H. Nie, Y. Xiong, J. Zou, H. Ning, Z. Wang, Z. Zhao, B. Z. Tang, *Adv. Funct. Mater.* 2018, **28**, 1803369.

27 R. N. Jones, *Chem. Rev.* 1947, **41**, 353-371.

28 J. Zhang, Y. Zhao, H. Xu, D. Zhang, Y. Miao, R. Shinar, J. Shinar, H. Wang, B. Xu, Y. Wu, *J. Mater. Chem. C* 2019, **7**, 10810-10817.

29 X. Tang, Q. Bai, T. Shan, J. Li, Y. Gao, F. Liu, H. Liu, Q. Peng, B. Yang, F. Li, P. Lu, *Adv. Funct. Mater.* 2018, **28**, 1705813.

30 Y. Pan, J. Huang, W. Li, Y. Gao, Z. Wang, D. Yu, B. Yang, Y. Ma, *RSC Adv*. 2017, **7**, 19576-19583.

31 L. S. Zhang, C. Wang, F. Shen, P. Lu, B. Yang, Y. Ma, *Adv. Optical Mater.* 2014, **2**, 892-901.

32 B. Zhang, H. Wu, Z. Wang, A. Qin, B. Z. Tang, *J. Mater. Chem. C* 2020, **8**, 4754-4762.

33 P. Han, C. Lin, D. Ma, A. Qin, B. Z. Tang, *ACS Appl. Mater. Interfaces* 2020, **12**, 46366-46372.

34 Y. Zhang, Z. Chen, J. Song, J. He, X. Wang, J. Wu, S. Chen, J. Qu, W.-Y. Wong, *J. Mater. Chem. C* 2019, **7**, 1880-1887.

35 C. Zhou, X. Zhang, G. Pan, X. Tian, S. Xiao, H. Liu, S. Zhang, B. Yang, *Org. Electron.* 2019, **75**, 105414.

36 X. Chen, Z. Yang, Z. Xie, J. Zhao, Z. Yang, Y. Zhang, M. P. Aldred, Z. Chi, Aldred, M. P.; Chi, Z. *Mater. Chem. Front.* 2018, **2**, 1017-1023.

37 T. I. Sutomu, I. Kitahar, S. Yamad, Y. Sanad, A. Sakurai, N. Tanak, T. Hase, S. Tobita, *Org. Biomol. Chem.* 2015, **13**, 1818-1828.

38 S.-Y. Yang, Y.-L. Zhang, A. Khan, Y.-J. Yu, S. Kumar, Z.-Q. Jiang, L.-S. Liao, *J. Mater. Chem. C* 2020, **8**, 3079-3087.